CrossMark

ORIGINAL

DFT/TDDFT study of electronic and optical properties of Surface-passivated Silicon nanocrystals, Si_n ($n = 20, 24, 26$ and 28)
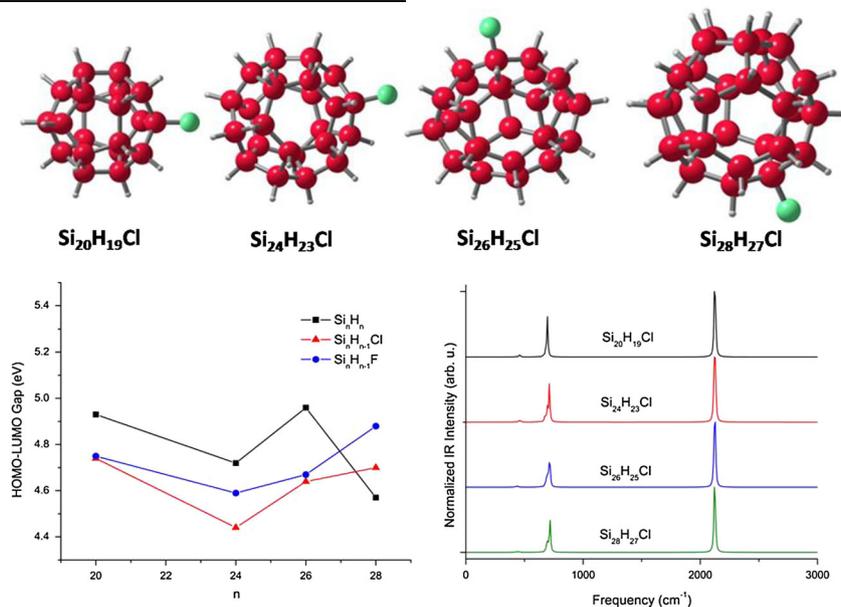
S. Chopra · B. Rai

Abstract Density functional theory and Time-dependent density functional theory (TDDFT)-based calculations were performed on surface-passivated Silicon nanocrystals (SPSNs) of different sizes. The surface passivation was achieved using H, F and Cl atoms. Various properties of the resulting optimized structures Si_nH_n, $Si_nH_{n-1}F$ and $Si_nH_{n-1}Cl$ ($n = 20, 24, 26$ and 28) like binding Energy, dipole moment, HOMO–LUMO gap, vibrational IR spectra and absorption wavelengths were determined. Surface passivation studies reveal that all the SPSNs are insulators and TDDFT study performed using two basis sets 6-31G and 6-31+G (d,p) shows that the maximum optical absorption of all the samples lie in the UV region, except for $Si_{28}H_{27}F$ SPSN which shows maximum absorption at ~ 588 nm. The absorption transitions in the Si_nH_n, $Si_nH_{n-1}F$ and $Si_nH_{n-1}Cl$ were characterized to be from pi→pi* transitions.

Graphical Abstract

Si$_{20}$H$_{19}$Cl   Si$_{24}$H$_{23}$Cl   Si$_{26}$H$_{25}$Cl   Si$_{28}$H$_{27}$Cl

S. Chopra (✉) · B. Rai
Department of Physics, AIAS, Amity University, Noida, India
e-mail: sidhusai@gmail.com

 Springer

Introduction

The field of research surrounding the optical and electrical
properties of semiconductor nanocrystals has witnessed an
enormous growth over the last decade [1–3]. Because of
being compatible with conventional microelectronics and
minimum feature size approaching to atomistic dimen-
sions, silicon-based molecular electronics has emerged as a
viable option [4, 5]. Freestanding silicon nanocrystals hold
great promise for a variety of applications such as photo-
voltaics [6–8], microelectronics [9, 10], bioimagings [11,
12], optoelectronics [13, 14] and photosensitizing [15, 16].
Furthermore, to design high density electronic devices for
molecular computers, electronic properties of small organic
molecules have been studied [17, 18]; thus, extended
studies for molecule–silicon junctions are also needed [19–
21]. Especially, in an approach to molecular electronics the
interconnection of organic molecules to semiconductors
plays a vital role. Strongly doped silicon has been proved
to be an excellent contact to interconnect to molecules,
even more robust than gold [22]. Recent efforts are already
oriented towards the characterization of hydrogen-passi-
vated silicon interfaces for the synthesis of molecular
electronic devices [23] as well as to study the effects
produced by metals on organic molecules laying on
hydrogen-passivated silicon.

Surface modification of silicon nanocrystals (Si NCs) is
carried out to prevent them from oxidation [24–29]. Kau-
zlarich et al. [19] synthesized Cl-passivated Si NCs at room
temperature in liquid phase and performed silanization,
alkylation, and alkoxylation to modify them and found that
the stability of Si NCs against oxidation dramatically
increased after surface modification [30–32]. However, it
was observed that no changes in photoluminescence (PL)
from Si NCs were induced by surface modification [30, 32].
However, in the work of Rogozhina et al. [35] the amini-
zation of Cl-passivated Si NCs by the use of butylamine led
to a redshift of the PL from Si NCs, which indicated that
surface chemistry effect should be taken into account in the
surface modification of Si NCs. Also, the sensitive depen-
dence of the electrical, optical and magnetic properties of
semiconductors on dopants has enabled an extensive range
of semiconductor technologies [36]. Several new applica-
tions that require the discrete character of a single dopant,
such as single spin devices in the area of quantum infor-
mation or single-dopant transistors, demand a further focus
on the properties of a specific dopant. It is well known that
when the semiconductor technologies move into the nan-
ometer-sized regime, dopants remain critical [37, 38].

The size dependence of the highest occupied molecular
orbital (HOMO) and the lowest unoccupied molecular
orbital (LUMO) gap is one of the fundamental signatures
of semiconductor nanocrystals or quantum dots, providing
many unique physical properties and attracting consider-
able attention in optoelectronics, spintronics, photovoltaic,
and biolabeling [39–45]. As the size of a semiconductor
cluster shrinks, its optical gap and dipole oscillator strength
increase with respect to the bulk value. Recently, many of
the size-dependent optical properties of various semi-
conductor nanocrystals have been measured and char-
acterized using several experimental methods [46–50].
Most of the theoretical effort has been devoted to calcu-
lations of the optical gap of semiconductor nanocrystals.
However, the emission energy is actually most often
measured and is usually more relevant for technological
applications. In general, the absorption gap is larger than
the emission gap; that is, light absorbed by semiconductor
clusters is red-shifted to longer wavelengths on emission.
This red shift is termed to as the Stokes shift, and its origin,
magnitude, and size dependence have been a notable
source of controversy in the recent literature, especially for
SiNCs. Some measurements have found size-dependent
Stokes shifts that decrease starting from 1.0 eV in small Si
clusters [51–53]. Most recent work has demonstrated that
single-walled carbon nanotubes when inserted into plants
(termed as plant nanobionics) actually augment the pho-
tosynthesis and biochemical sensing [54].

In the present study, we have performed density func-
tional theory (DFT) and time-dependent density functional
theory (TDDFT) calculations on surface-passivated Silicon
nanocrystals (SPSNs) using hydrogen, fluorine and chlo-
rine atoms as surface passivants. All the SPSNs were then
optimized for the lowest energy configurations. Several
properties of the SPSNs, like binding energy, energy gap
(HOMO–LUMO), dipole moment and absorption wave-
lengths were determined using the DFT and TDDFT cal-
culations. To aid identification, infrared spectra have also
been calculated.

Methodology

The present calculations are performed using DFT and
TDDFT. Self-consistent field (SCF) electronic structure
calculations have been carried out on all the surface-pas-
sivated silicon nanocrystals (SPSNs), Si_nH_n, $Si_nH_{n-1}F$ and
$Si_nH_{n-1}Cl$ with $n = 20, 24, 26$ and 28 (in total 12). Doped
silicon-based nano-clusters of the same size happen to be
promising nano-units in the emerging (low-dimensional)
nano-opto-electronics [55]. The Pople′s N-31G split va-
lence basis set 6-31G was used for all structures. Geometry
optimizations were carried out using internal coordinates

Fig. 1 Different Optimized SPSNs (*Red* Silicon, *Gray* Hydrogen, *Green* Chlorine, *Purple* Fluorine)

$Si_{20}H_{20}$ $Si_{24}H_{24}$ $Si_{26}H_{26}$ $Si_{28}H_{28}$

$Si_{20}H_{19}Cl$ $Si_{24}H_{23}Cl$ $Si_{26}H_{25}Cl$ $Si_{28}H_{27}Cl$

$Si_{20}H_{19}F$ $Si_{24}H_{23}F$ $Si_{26}H_{25}F$ $Si_{28}H_{27}F$
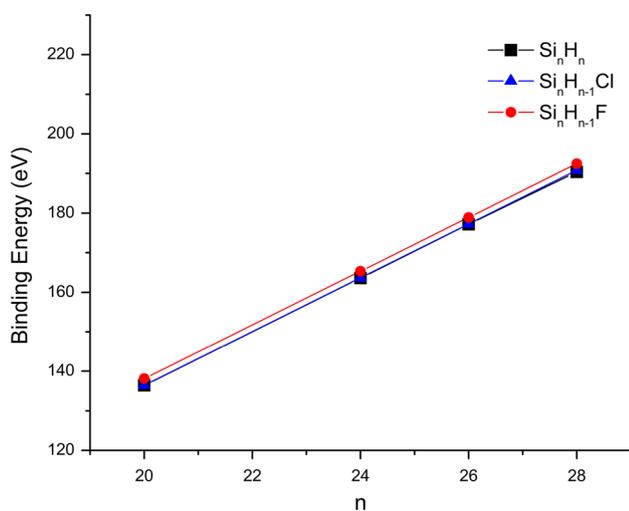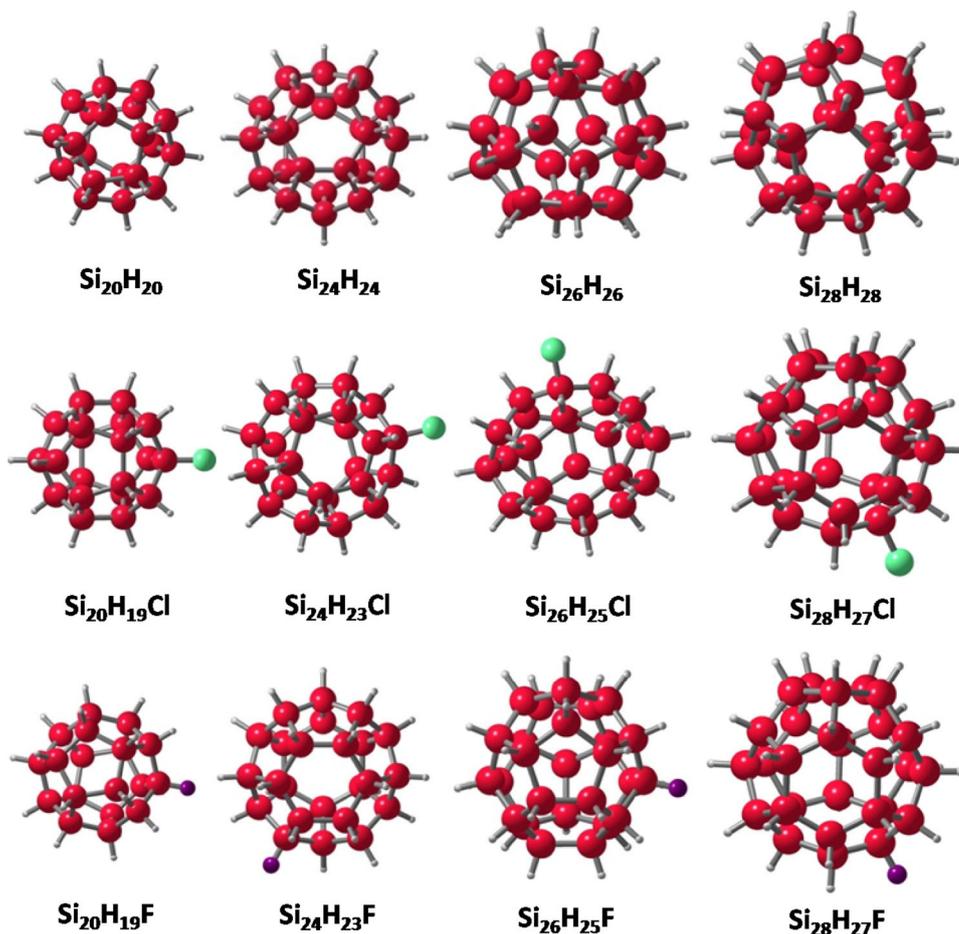

Fig. 2 Variation of Binding Energy with the index '*n*' of different SPSNs
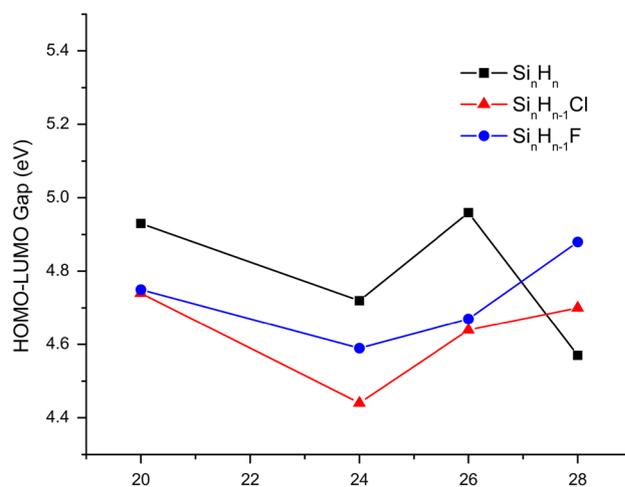

Fig. 3 HOMO–LUMO Gap variation with the index '*n*' of different SPSNs

and with a convergence limit of 10^{-7} hartree on the total energy. All the structures were built using the Avogadro package [56], and then the optimized structures were obtained by first relaxing the structures using the Steepest Descent algorithm in the Avogadro, without any symmetry constraints. It was followed by a more accurate calculation carried out using Becke's three parameter functional with the Lee–Yang–Parr correlation functional (B3LYP) level of theory [57, 58]. Similar DFT methods were successfully
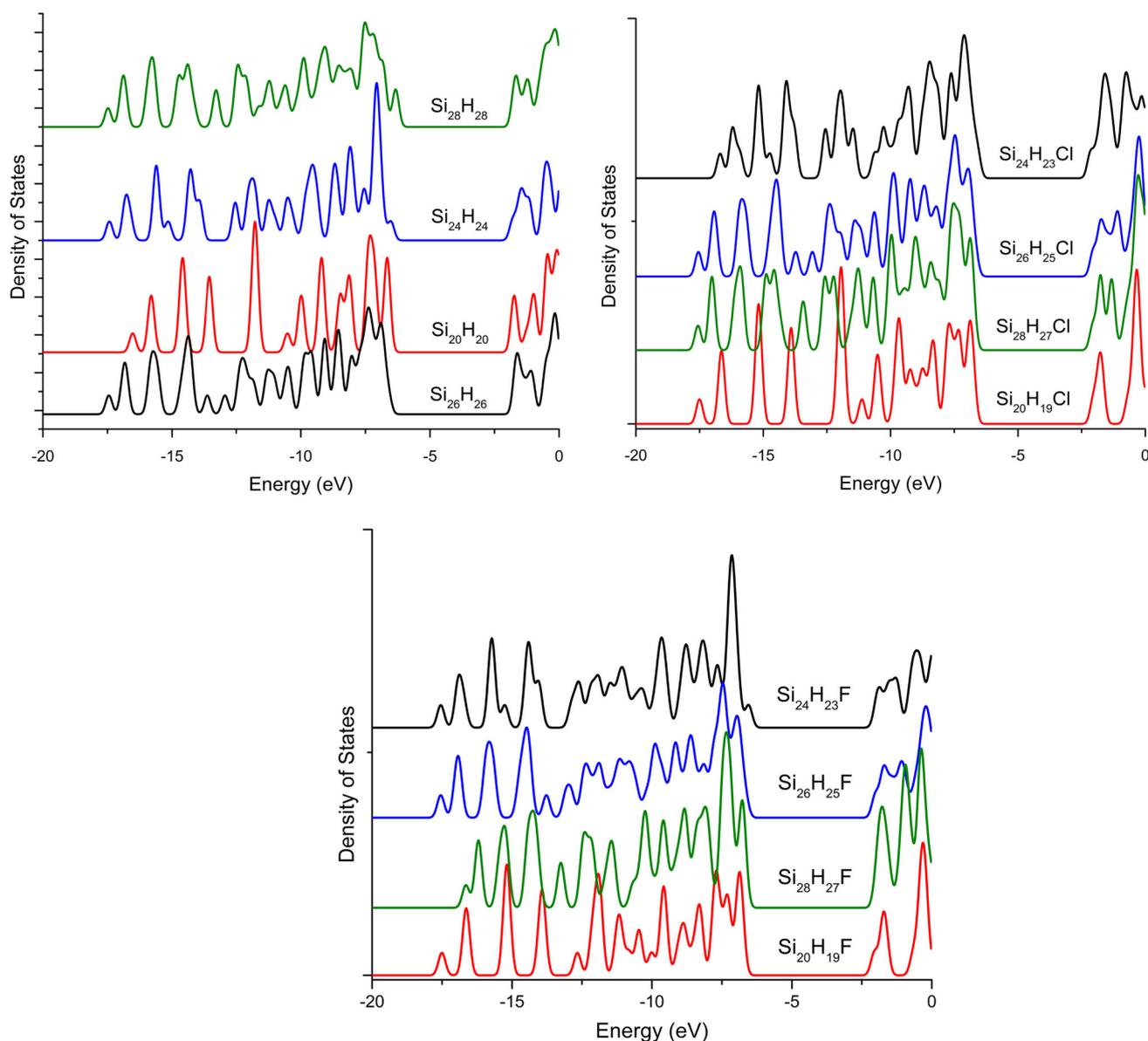
Fig. 4 Density of States of all SPSNs arranged in the order of increasing gap between virtual and occupied orbitals, from top to bottom

used to calculate the electronic properties of carbon clusters (fullerenes), similar in shape, symmetry and sizes [59]. Electronic properties were calculated from the SCF electronic energy and the orbital energy values. All theoretical calculations have been performed with the FIREFLY version 8.0.1 program code [60, 61]. The optimized geometries were confirmed as minima on the potential energy surface (PES) by evaluating the hessian and checking for the presence of all real frequencies. The density of states plots was extracted from the DFT calculations with the help of Gausssum v3.0 package [62]. The electronic transitions between occupied and unoccupied states were calculated at Restricted Hartree–Fock (RHF) and TDDFT/B3LYP level of theory using basis sets 6-31G and 6-31+G

(d,p), with 100 singlet excited states that result in the UV absorption spectra and the main orbitals contributing to the transitions. The optimized ground state configurations of all the SPSNs were used as starting configurations for the TDDFT calculations. TDDFT calculations were performed with no symmetry constraints. A very similar approach has been used in a recent TDDFT study on silicon-based clusters [63].

Results and discussions

In the current study, silicon nanocrystals surface passivated with H, Cl and F atoms (Si_nH_n, $Si_nH_{n-1}F$ and $Si_nH_{n-1}Cl$
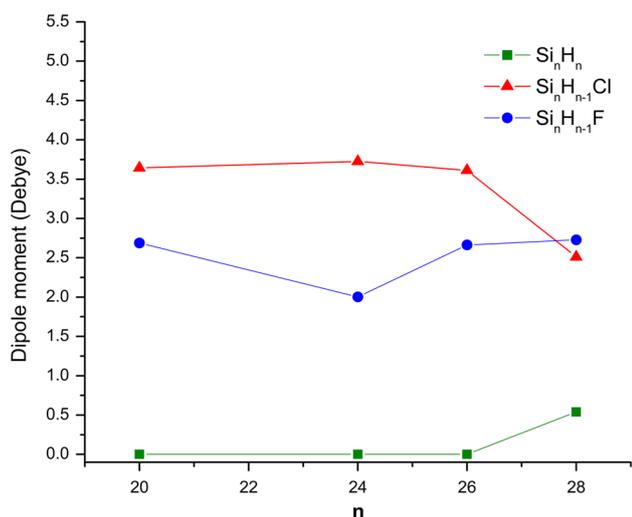
Fig. 5 Dipole moment variation with the index 'n' of different SPSNs

with $n = 20$, 24, 26 and 28) each have been considered. All the optimized structures (SPSNs) arranged categorically in the ascending order of their number of atoms can be seen in Fig. 1.

The binding energy is calculated using general Eq. (1):

$$\text{Binding energy (eV)} = [(N_H \times E_H + N_{Si} \times E_{Si} + E_X) - E_{SPSN}] \quad (1)$$

where, E_{SPSN} is the total energy of the SPSN; N_H, N_{Si} are the number of hydrogen and silicon atoms, and E_H, E_{Si} are energies of these individual atoms. E_x is the energy of individual fluorine or chlorine atoms. The E_x term vanishes in Eq. (1) for the Si_nH_n SPSNs.

The Binding Energy (in eV) plots shown in Fig. 2 display the stabilities of the SPSNs (Si_nH_n, $Si_nH_{n-1}F$ and $Si_nH_{n-1}Cl$) with the increasing size $n = 20$, 24, 26 and 28. It has been consistently found that for all the SPSNs, the binding energy increases with the increasing value of 'n'. It demonstrates that the formation of larger clusters is favored. In the present study, most favorable SPSNs are found to be $Si_{28}H_{28}$, $Si_{28}H_{27}Cl$ and $Si_{28}H_{27}F$.

The HOMO–LUMO gaps/electronic gaps (in eV) were determined for all the SPSNs. As observed from the Fig. 3, it can be noted the HOMO–LUMO gap varies between 4.57–4.96, 4.44–4.74 and 4.59–4.88 eV for Si_nH_n, $Si_nH_{n-1}Cl$ and $Si_nH_{n-1}F$ SPSNs. This band gap variation demonstrates the insulating nature of all the SPSNs, indicating the difficulty of transition of electrons from HOMO to LUMO orbitals. Additionally it can be extrapolated that the surface passivation with H, F and Cl atoms does not seem to play a major role in the conductivity of the SPSNs. It is to be noted that the HOMO–LUMO gaps are however underestimated in DFT calculations. In addition, it is to be noted that much smaller gaps ($\sim$1.5 eV) have recently

been reported for hydrogenated silicon clusters of quite comparable size [64, 65]. However, these small gaps resulted from the non-tetrahedral and over-coordinated structures of those clusters.

The density of states of all the SPSNs is shown in Fig. 4. It is clearly seen that the spectrum of $Si_{24}H_{23}Cl$ is the narrowest (between the virtual and occupied orbitals), while the spectrum of $Si_{26}H_{26}$ is the widest, indicating that HOMO–LUMO gap of $Si_{24}H_{23}Cl$ is smallest and that of $Si_{26}H_{26}$ is highest.

The Fig. 5 shows variation of the dipole moment of all the SPSNs. The dipole moments were found to vary from 0.0 to 0.54, 2.5 to 3.73 and 2.0 to 2.73 Debye for Si_nH_n, $Si_nH_{n-1}Cl$ and $Si_nH_{n-1}F$ SPSNs, respectively. The maximum dipole moment/polarity has been found for the $Si_{28}H_{28}$, $Si_{24}H_{23}Cl$ and $Si_{28}H_{27}F$ in their categories, indicating the most polar nature. The $Si_{20}H_{20}$ SPSN has been found to be non-polar.

In this work, IR spectra have been calculated to validate the vibrational structures of Si_nH_n, $Si_nH_{n-1}Cl$ and $Si_nH_{n-1}F$ SPSNs, respectively. All the IR spectra can be seen in Fig. 6, where the IR intensities are normalized. For all the SPSNs, Si–Si stretching fundamental frequencies were observed in the range 692–717 cm^{-1} and Si–H stretching frequencies at 2121 cm^{-1} (Fig. 6a, b, c), which is in agreement with the work by Boo et al. [66]. In the $Si_nH_{n-1}Cl$ SPSNs the Si–Cl fundamental frequency was observed in the range of 438– 461 cm^{-1} (Fig. 6b). For the $Si_nH_{n-1}F$ SPSNs, we observed Si–H stretching fundamental frequency at 2121 cm^{-1} which is same as that for Si_nH_n but Si–Si stretching fundamental frequency shifted in the range 700–716 cm^{-1}. Unlike the work of Lucovsky et al. [67] who reported the Si–F stretching mode frequencies around 935 cm^{-1} and Si–F bond bending frequencies below 400 cm^{-1}, we observed weak shoulder peaks of Si–F bond with fundamental frequencies in the range 763–772 cm^{-1} (Fig. 6c). It is important to note from the figures that the intensities of Si–Cl and Si–F bonds are very less as compared to Si–H and Si–Si signature peaks, due to the fact that there are single Cl and F passivants atoms in all the SPSNs.

The maximum absorption wavelengths were also calculated for all the optimized SPSNs. TDDFT calculations show that all the SPSNs exhibit maximum UV absorption in the wavelength range 180–350 nm which constitutes the UV-B and UV-C regions. Table 1 comparatively lists the wavelength corresponding to the maximum absorbance (λ_{max}) and the maximum oscillator strengths, for two basis sets 6-31G and 6-31+G (d,p) and provides the molar absorption coefficients (ε_{max}) along with the major contributions with transition probabilities greater than 10 % for all the SPSNs, for larger basis set 6-31+G (d,p). It is clearly seen from the Table 1 that overall the λ_{max} values get red-shifted and oscillator strengths (f) have reduced/corrected
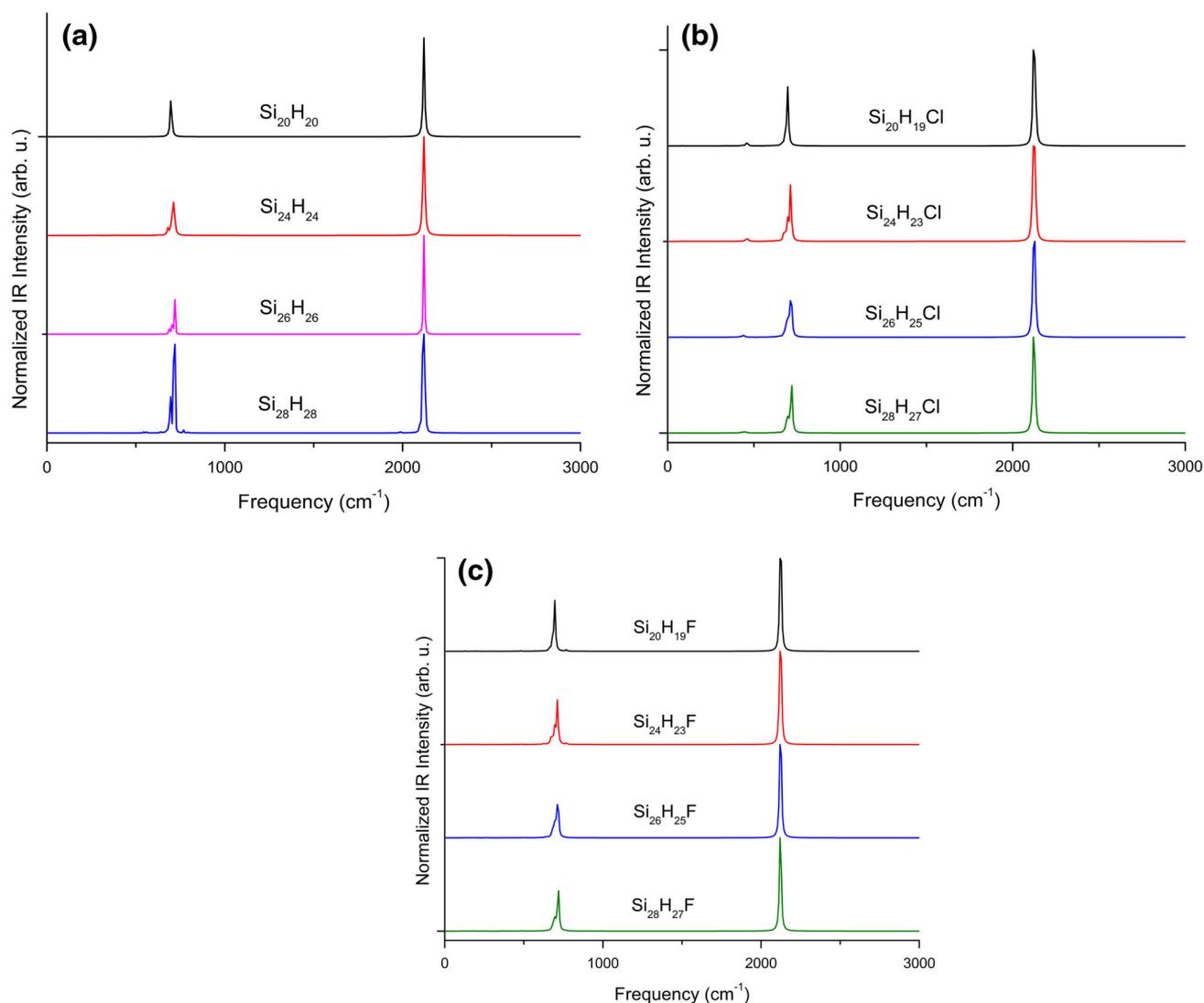
Fig. 6 IR vibrational spectra of all the SPSNs indicating the signature peaks of Si–H, Si–Si, Si–F and Si–Cl bonds

with the larger basis set. The further discussion on optical absorption will be based on the 6-31+G (d,p) basis set. It is known that the oscillator strength is proportional to absorbance in a UV–Visible absorption spectrum. The λ_{max} values are found in the range 248.455–588.323 nm for all the SPSNs indicating a strong absorption capability of these SPSNs in ultraviolet region except for $Si_{28}H_{27}F$ SPSN which has maximum absorption at 588.323 nm. In the case of Si_nH_n SPSNs, the maximum molar absorption coefficient (ε_{max}) is found for $Si_{24}H_{24}$ ($\sim$6000 M^{-1}cm^{-1}) indicating the orbital transition to be from pi-bonding to pi-antibonding orbital transition (pi$\rightarrow$pi*). In case of the $Si_nH_{n-1}F$ SPSNs, pi$\rightarrow$pi* transition is observed as the intense peaks with highest ε_{max} ($\sim$21000 M^{-1}cm^{-1}) for $Si_{28}H_{27}F$. For $Si_nH_{n-1}Cl$ SPSNs, again the pi$\rightarrow$pi* transition is assigned to the strong absorption with the highest ε_{max} ($\sim$6200 M^{-1}cm^{-1}) for $Si_{24}H_{23}Cl$. There was no

consistent shift found in the λ_{max} found for all the SPSNs with increasing size. In all the SPSNs, lowest absorption wavelengths were found for the SPSNs with $n = 20$, and maximum absorption wavelengths were found for $n = 24$ SPSNs. It is also to be noted from Table 1, that the major contributions to the transitions in all the SPSNs are from the deeper levels and not from the surface states (HOMO, LUMO). Moreover, several orbitals are playing role in the transitions. The highest contributions were found from H-11->L+2 (61 %) in case of $Si_{28}H_{28}$, H-10->L+2 (44 %) for $Si_{24}H_{23}F$ and H-4->L+4 for $Si_{24}H_{23}Cl$.

Conclusion

The binding energy variations show that all the SPSNs (Si_nH_n, $Si_nH_{n-1}F$ and $Si_nH_{n-1}Cl$ with $n = 20$, 24, 26 and

Table 1 TDDFT computed maximum absorption wavelengths (λ_{max}), oscillator strengths (f), molar absorption coefficients (ε_{max}) and orbital transitions (for 6-31+G (d,p) basis set) of all the SPSNs

SPSN	6-31G[a]		6-31+G (d,p)[b]			
	λ_{max} (nm)	f	λ_{max} (nm)	f	ε_{max} (M^{-1}cm^{-1}) ($\sim$)	Major contributions (>10 %)
$Si_{20}H_{20}$	230.324	0.032	248.455	0.023	5000	H-12→L+2 (24 %), H-11→L+1 (14 %), H-9→L+3 (26 %)
$Si_{24}H_{24}$	229.763	0.051	263.657	0.026	6000	H-10→L+1 (12 %), H-4→L+4 (25 %), H-3→L+5 (25 %)
$Si_{26}H_{26}$	235.294	0.036	256.373	0.024	3400	H-8→L+3 (24 %), H-7→L+2 (24 %)
$Si_{28}H_{28}$	236.799	0.009	257.046	0.010	4400	H-13→L+1 (20 %), H-11→L+2 (61 %)
$Si_{20}H_{19}Cl$	228.001	0.030	250.881	0.014	5200	H-13→L+3 (16 %), H-12→L+3 (21 %), H-11→L+2 (20 %)
$Si_{24}H_{23}Cl$	258.921	0.006	266.407	0.008	6200	H-9→L+2 (13 %), H-5→L+4 (12 %), H-4→L+4 (32 %)
$Si_{26}H_{25}Cl$	234.488	0.016	258.005	0.007	3600	H-12→L+3 (12 %), H-8→L+3 (18 %), HOMO→L+11 (11 %)
$Si_{28}H_{27}Cl$	266.431	0.009	259.074	0.007	3500	H-10→L+5 (13 %), H-9→L+6 (31 %)
$Si_{20}H_{19}F$	232.286	0.015	249.935	0.014	5000	H-12→L+3 (32 %), H-11→L+2 (32 %)
$Si_{24}H_{23}F$	242.368	0.013	261.989	0.015	5600	H-10→L+2 (44 %), H-4→L+5 (15 %)
$Si_{26}H_{25}F$	232.547	0.019	257.919	0.007	3800	H-11→L+3 (32 %), H-8→L+3 (23 %)
$Si_{28}H_{27}F$	562.323	0.098	588.218	0.071	21000	H-10→L+1 (24 %)

28) with higher sizes (corresponding to 'n') are most favorable. HOMO–LUMO Gap calculations show that all the SPSNs demonstrate an insulating nature. Slight variations in the band gaps with lowest gap (4.44 eV) for the $Si_{24}H_{23}Cl$ SPSN and highest for $Si_{26}H_{26}$ (4.96 eV) were found. This could indicate that there is no significant effect of surface passivation or even the cluster size on the conductivity of all the SPSNs.

The maximum absorption wavelengths were obtained from TDDFT calculations. The maximum wavelength absorption for all the SPSNs was found to lie in the UV region except for $Si_{28}H_{27}F$ SPSN which has maximum absorption at 588.323 nm. The absorption transitions in the Si_nH_n, $Si_nH_{n-1}F$ and $Si_nH_{n-1}Cl$ were characterized to be from pi→pi* transitions. All the SPSNs studied in the present study could be effectively used in the applications of optical filters, photodetectors and plant nanobionics (to enhance the solar energy capture).

References

1. Chen, C.C., Herhold, A.B., Johnson, C.S., Alivisatos, A.P.: Size dependence of structural metastability in semiconductor nanocrystals. Science **276**, 398 (1997)
2. Chan, W.C.W., Nie, S.: Quantum dot bioconjugates for ultra-sensitive nonisotopic detection. Science **281**, 2016 (1998)
3. Yoffe, A.D.: Semiconductor quantum dots and related systems: electronic, optical, luminescence and related properties of low dimensional systems. Adv. Phys. **50**, 1–208 (2001)
4. Basu, R., Tovar, J.D., Hersam, M.C., Basu, R., Tovar, J.D., Hersam, M.C.: Scanning tunneling microscopy study of single molecule motion on the Si (100)- 2 × 1 surface. J. Vac. Sc. Tech. B **23**(4), 1785–1789 (2005)
5. Rakshit, T., Liang, G.-C., Ghosh, A.K.G., Datta, S.: Silicon-based molecular electronics. Nano. Lett. **4**(10), 1803–1807 (2004)
6. Pi, X.D., Li, Q., Li, D., Yang, D.: Spin-coating silicon-quantum-dot ink to improve solar cell efficiency. Sol. Energy Mater. Sol. Cells **95**, 2941–2945 (2011)
7. Wurfl, I.P., Hao, X., Gentle, A., Kim, D.-H., Conibeer, G., Green, M.A.: Si nanocrystal pin diodes fabricated on quartz substrates for third generation solar cell applications. Appl. Phys. Lett. **95**, 153506 (2009)
8. Kim, S., Jeon, K., Lee, J.C., Swihart, M.T., Yang, M.: Enhanced performance of a polymer solar cell upon addition of free-standing, freshly etched photoluminescent silicon nanocrystals. Appl. Phys. Express **5**, 022302 (2012)
9. Ding, Y.P., Dong, Y., Bapat, A., Nowak, J.D., Carter, C.B., Kortshagen, U.R., Campbell, S.A.: Single nanoparticle semiconductor devices. IEEE Trans. Electron Devices **53**, 2525–2531 (2006)
10. Huang, S., Banerjee, S., Tung, R.T., Oda, S.: Electron trapping, storing, and emission in nanocrystalline Si dots by capacitance–voltage and conductance–voltage measurements. J. Appl. Phys. **93**, 576–581 (2003)
11. He, Y., Zhong, Y.L., Peng, F., Wei, X.P., Su, Y.Y., Lu, Y.M., Su, S., Gu, W., Liao, L.S., Lee, S.T.: One-Pot microwave synthesis of water-dispersible, ultraphoto- and pH-Stable, and highly fluorescent silicon quantum dots. J. Am. Chem. Soc. **133**, 14192–14195 (2011)
12. Erogbogbo, F., Yong, K.T., Roy, I., Hu, R., Law, W.C., Zhao, W., Ding, H., Wu, F., Kumar, R., Swihart, M.T., Prasad, P.N.: In vivo targeted cancer imaging, sentinel lymph node mapping and multi-channel imaging with biocompatible silicon nanocrystals. ACS Nano. **5**, 413–423 (2011)
13. Yuan, Z., Anopchenko, A., Daldosso, N., Guider, R., Navarro-Urrios, D., Pitanti, A., Spano, R., Pavesi, L.: Silicon nanocrystals as an enabling material for silicon photonics. Proc. IEEE **97**, 1250–1268 (2009)

14. Walters, R.J., Bourianoff, G.I., Atwater, H.A.: Field-effect electroluminescence in silicon nanocrystals. Nat. Mater. **4**, 143–146 (2005)

15. Kovalev, D., Fujii, M.: Silicon nanocrystals: photosensitizers for oxygen molecules. Adv. Mater. **17**, 2531–2544 (2005)

16. Pi, X.D., Zalloum, O.H.Y., Wojcik, J., Knights, A.P., Mascher, P., Todd, A.D.W., Simpson, P.J.: Formation and oxidation of Si nanoclusters in Er-doped Si-rich SiOx. J. Appl. Phys. **97**, 096108 (2005)

17. Boyen, H.G., Ziemann, P., Wiedwald, U., Ivanova, V., Kolb, D.M., Sakong, S., Gross, A., Romanyuk, A., Büttner, M., Oelhafen, P.: Local density of states effects at the metal-molecule interfaces in a molecular device. Nat. Mater. **5**(5), 394–399 (2006)

18. Zhang, C., Du, M.-H., Cheng, H.-P., Zhang, X.G., Roitberg, A.E., Krause, J.L.: Coherent electron transport through an azobenzene molecule: a light-driven molecular switch. Phys. Rev. Lett. **92**(15), 158301 (2004)

19. Xue, Y.Q., Ratner, M.A.: First-principles calculations of intrinsic defects in Al2O3. Phys. Rev. B **68**(11), 085110 (2003)

20. Xue, Y.Q., Ratner, M.A.: Microscopic study of electrical transport through individual molecules with metallic contacts. I. Band lineup, voltage drop, and high-field transport. Phys. Rev. B **68**, 115406 (2003)

21. Herrera, C., Seminario, J.M.: Study of nano-structured silicon-phenyl nanoclusters towards single molecule sensing. Int J High Speed Electron. Syst. **17**(2), 327–338 (2007)

22. Chen, B., Flatt, A.K., Jian, H., Hudson, J.L., Tour, J.M.: Molecular grafting to silicon surfaces in air using organic triazenes as stable diazonium sources and HF as a constant hydride-passivation source. Chem. Mater. **17**(19), 4832–4836 (2005)

23. Cleri, F., Letardi, S., Delerue, C.: Screening and surface states in molecular monolayers adsorbed on silicon surfaces. J. Phys. Chem. B **113**, 3244 (2006)

24. Veinot, J.G.C., Kelly, J.A., Shukaliak, A.M., Fleischauer, M.D.: Size-dependent reactivity in hydrosilylation of silicon nanocrystals. J. Am. Chem. Soc. **133**, 9564–9571 (2011)

25. Gupta, A., Swihart, M.T., Wiggers, H.: Luminescent colloidal dispersion of silicon quantum dots from microwave plasma synthesis: exploring the photoluminescence behavior across the visible spectrum. Adv. Funct. Mater. **19**, 696–703 (2009)

26. Hessel, C.M., Reid, D., Panthani, M.G., Rasch, M.R., Goodfellow, B.W., Wei, J., Fujii, H., Akhavan, V., Korgel, B.A.: Synthesis of ligand-stabilized silicon nanocrystals with size-dependent photoluminescence spanning visible to near-infrared wavelengths. Chem. Mater. **24**, 393–401 (2011)

27. Shiohara, A., Hanada, S., Prabakar, S., Fujioka, K., Lim, T.H., Yamamoto, K., Northcote, P.T., Tilley, R.D.: Chemical reactions on surface molecules attached to silicon quantum dots. J. Am. Chem. Soc. **132**, 248–253 (2010)

28. Baldwin, R.K., Zou, J., Pettigrew, K.A., Yeagle, G.J., Britt, R.D., Kauzlarich, S.M.: The preparation of a phosphorus doped silicon film from phosphorus containing silicon nanoparticles. Chem. Commun. **6**, 658–660 (2006)

29. Baldwin, R.K., Pettigrew, K.A., Ratai, E., Augustine, M.P., Kauzlarich, S.M.: Solution reduction synthesis of surface stabilized silicon nanoparticles. Chem. Commun. **17**, 1822–1823 (2002)

30. Zou, J., Kauzlarich, S.M.: Functionalization of silicon nanoparticles via silanization: alkyl, halide and ester. J. Cluster Sci. **19**, 341–355 (2008)

31. Mayeri, D., Phillips, B.L., Augustine, M.P., Kauzlarich, S.M.: NMR study of the synthesis of alkyl-terminated silicon nanoparticles from the reaction of SiCl4 with the zintl salt. NaSi. Chem. Mater. **13**, 765–770 (2001)

32. Pettigrew, K.A., Liu, Q., Power, P.P., Kauzlarich, S.M.: Solution synthesis of alkyl- and alkyl/alkoxy-capped silicon nanoparticles via oxidation of Mg$_2$Si. Chem. Mater. **15**, 4005–4011 (2003)

33. Rogozhina, E., Belomoin, G., Smith, A., Abuhassan, L., Barry, N., Akcakir, O., Braun, P.V., Nayfeh, M.H.: Si–N linkage in ultrabright, ultrasmall Si nanoparticles. Appl. Phys. Lett. **78**, 3711–3713 (2001)

34. Sze, S.M., Ng, K.K.: Physics of Semiconductor Devices. Wiley, New York (2006)

35. Norris, D.J., Efros, A.L., Erwin, S.C.: Review: doped nanocrystals. Science **319**, 1776–1779 (2008)

36. Fukata, N.: Impurity doping in silicon nanowires. Adv. Mater. **21**, 2829–2832 (2009)

37. Schmidt, M.E., Blanton, S.A., Hines, M.A., Sionnest, P.G.: Size-dependent two-photon excitation spectroscopy of CdSe nanocrystals. Phys. Rev. B **53**, 12629 (1996)

38. Banin, U., Cerullo, G., Guzelian, A.A., Bardeen, C.J., Alivisatos, A.P., Shank, C.V.: Quantum confinement and ultrafast dephasing dynamics in InP nanocrystals. Phys. Rev. B **55**, 7059 (1997)

39. Harbold, J.M., Du, H., Krauss, T.D., Cho, K.-S., Murray, C.B., Wise, F.W.: Time-resolved intraband relaxation of strongly-confined electrons and holes in colloidal PbSe nanocrystals. Phys. Rev. B **72**, 195312 (2005)

40. Scholes, G.D., Rumbles, G.: Excitons in nanoscale systems. Nat. Mater. **5**, 683 (2006)

41. Klimov, V.I., Ivanov, S.A., Nanda, J., Achermann, M., Bezel, I., McGuire, J.A., Piryatinski, A.: Single-exciton optical gain in semiconductor nanocrystals. Nature **447**, 441 (2007)

42. Rogach, A.L., Gaponik, N., Lupton, J.M., Bertoni, C., Gallardo, D.E., Dunn, S., Pira, N.L., Paderi, M., Repetto, P., Romanov, S.G., Dwyer, C.O., Torres, C.M.S., Eychmueller, A.: Light-emitting diodes with semiconductor nanocrystals. Angew. Chem. Int. Ed. Engl. **47**, 6538 (2008)

43. Franceschetti, A., Fu, H., Wang, L.W., Zunger, A.: Many-body pseudopotential theory of excitons in InP and CdSe quantum dots. Phys. Rev. B **60**, 1819 (1999)

44. Murray, C.B., Kagan, C.R., Bawendi, M.G.: Self-organization of CdSe nanocrystallites into three-dimensional quantum dot superlattices. Science **270**, 1335 (1995)

45. Marzin, J.Y., Gerard, J.M., Izrael, A., Barrier, D., Bastard, G.: Photoluminescence of Single InAs Quantum Dots Obtained by Self-Organized Growth on GaAs. Phys. Rev. Lett. **73**, 716 (1994)

46. Furukawa, S., Migasato, T.: Quantum size effects on the optical band gap of microcrystalline Si:H. Phys. Rev. B **38**, 5726 (1988)

47. Wilson, W.L., Szajowski, P.F., Brus, L.E.: Quantum Confinement in Size-Selected. Surface-Oxidized Silicon Nanocrystals. Science **262**, 1242 (1993)

48. Schuppler, S., Friedman, S.L., Marcus, M.A., Adler, D.L., Xie, Y.H., Ross, F.M., Harris, T.D., Brown, W.L., Chabal, Y.J., Brus, L.E., Citron, P.H.: Dimensions of luminescent oxidized and porous silicon structures. Phys. Rev. Lett. **72**, 2648 (1994)

49. Holmes, J.D., Ziegler, K.J., Doty, R.C., Pell, L.E., Johnston, K.P., Korgel, B.A.: Highly luminescent silicon nanocrystals with discrete optical transitions. J. Am. Chem. Soc. **123**, 3743 (2001)

50. Baldwin, R.K., Pettigrew, K.A., Garno, J.C., Power, P.P., Liu, G.Y., Kauzlarich, S.M.L.: Room temperature solution synthesis of alkyl-capped tetrahedral shaped silicon nanocrystals. J. Am. Chem. Soc. **124**, 1150–1151 (2002)

51. Kanemitsu, Y., Okamoto, S.: Phonon structures and Stokes shift in resonantly excited luminescence of silicon nanocrystals. Phys. Rev. B **58**, 9652 (1998)

52. Garrido, B., Lopez, M., Gonzalez, O., Rodriguez, A.P., Morante, J.R., Bonafos, C.: Correlation between structural and optical properties of Si nanocrystals embedded in SiO2: the mechanism

of visible light emission. Appl. Phys. Lett. **77**(20), 3143–3145 (2000)

53. Belomoin, G., Therrein, J., Nayfeh, M.: Oxide and hydrogen capped ultrasmall blue luminescent Si nanoparticles. Appl. Phys. Lett. **77**, 779 (2000)

54. Giraldo, J.P., Landry, M.P., Faltermeier, S.M., McNicholas, T.P., Iverson, N.M., Boghossian, A.A., Reuel, N.F., Hilmer, A.J., Sen, F., Brew, J.A., Strano, M.S.: Plant nanobionics approach to augment photosynthesis and biochemical sensing. Nat. Mater. **13**, 400–408 (2014)

55. Gueorguiev, G.K., Stafström, S., Hultman, L.: Nano-wire formation by self-assembly of silicon–metal cage-like molecules. Chem. Phys. Lett. **458**(1–3), 170–174 (2008)

56. Hanwell, M.D., Curtis, D.E., Lonie, D.C., Vandermeersch, T., Zurek, E., Hutchison, G.R.: Avogadro: an open-source molecular builder and visualization tool. Version 1.1.0. http://avogadro.openmolecules.net. J. Cheminformatics. **4**, 17 (2012)

57. Lee, C., Yang, W., Parr, R.G.: Phys. Rev. B **37**, 785–789 (1988)

58. Becke, A.D.: Density-functional thermochemistry. III. The role of exact exchange. J. Chem. Phys. **98**, 5648–5652 (1993)

59. Gueorguiev, G.K., Pacheco, J.M.: Structural and electronic properties of C-36. J. Chem. Phys. **114**(14), 6068–6071 (2001)

60. Granovsky, A. A.: Firefly version 8.0.1. http://classic.chem.msu.su/gran/firefly/index.html

61. Schmidt, M.W., Baldridge, K.K., Boatz, J.A., Elbert, S.T., Gordon, M.S., Jensen, J.H., Koseki, S., Matsunaga, N., Nguyen, K.A., Su, S., Windus, T.L., Dupuis, M., Montgomery, J.A.: General atomic and molecular electronic structure system. J. Comput. Chem. **14**, 1347–1363 (1993)

62. O'Boyle, N.M., Tenderholt, A.L., Langner, K.M.: Cclib: a library for package-independent computational chemistry algorithms. J. Comp. Chem. **29**, 839–845 (2008)

63. Oliveira, M.I.A., Rivelino, R., de Brito Mota, F., Gueorguiev, G.K.: Optical properties and quasiparticle band gaps of transition-metal atoms encapsulated by silicon cages. J. Phys. Chem. C **118**(10), 5501–5509 (2014)

64. Vach, H.: Ultrastable silicon nanocrystals due to electron delocalization. Nano Lett. **11**, 5477–5481 (2011)

65. Vach, H.: Symmetric and irregular aromatic silicon nanoclusters. Phys. Lett. **614**, 199–203 (2014)

66. Boo, B.H.: Infrared and Raman Spectroscopic Studies Tris (trimethylsilyl) silane Derivatives of (CF3)(3) Si)(3) Si-X [X = H, Cl, OH, CH3, OCH3, Si (CH3)(3)]: Vibrational Assignments by Hartree-Fock and Density-functional theory calculations. J. Korean Phys. Soc. **59**(5), 3192–3200 (2011)

67. Lucovsky, G., Yang, H.: Fluorine Atom Induced Decreases to the Contribution of Infrared Vibrations to the Static Dielectric Constant of Si-O-F Alloy Films. J. Vac. Sci. Technol., A **15**(3), 836–843 (1997)